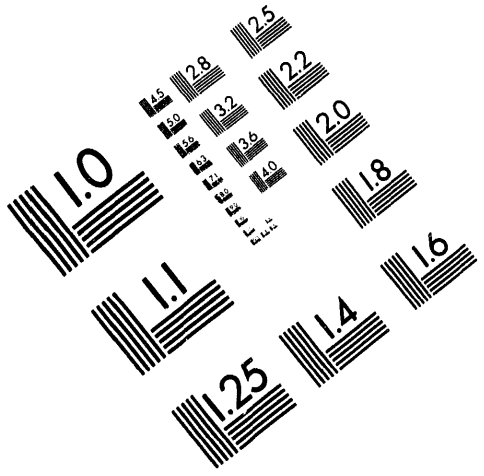

Association for Information and Image Management
1100 Wayne Avenue, Suite 1100
Silver Spring, Maryland 20910
301/587-8202

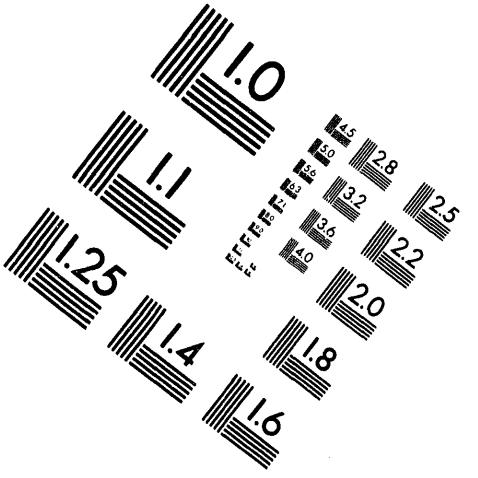

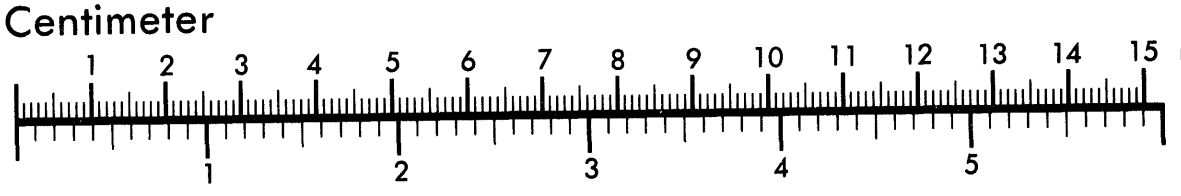

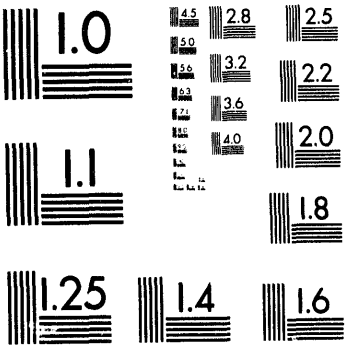

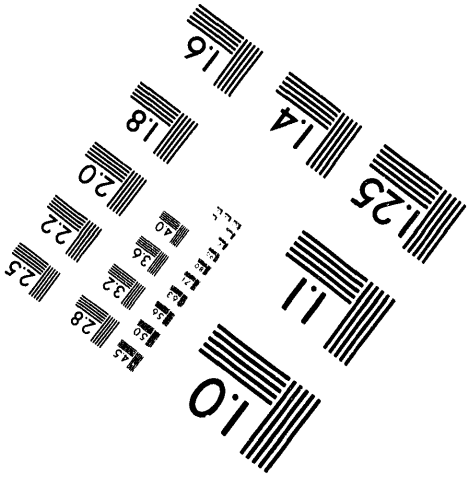

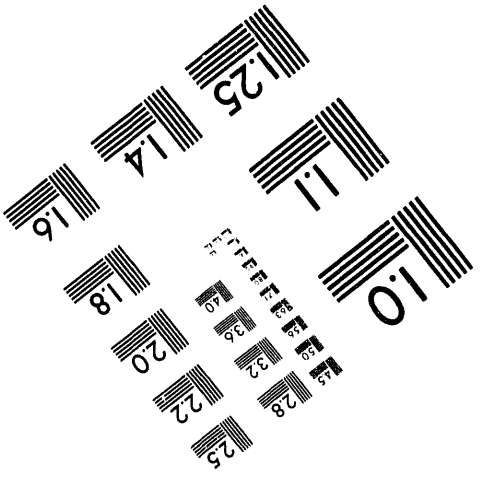

MANUFACTURED TO AIIM STANDARDS
BY APPLIED IMAGE, INC.

1 of 1

Conf-940616--1
SAND94-0506C

Microstructures of $InAs_{1-x}Sb_x$ (x = 0.07-0.14) Alloys and Strained-Layer Superlattices

D. M. Follstaedt, R. M. Biefeld, S. R. Kurtz and K. C. Baucom
Sandia National Laboratory
Albuquerque, NM 87185-1056

Abstract

Growth of $InAs_{1-x}Sb_x$ alloys by MOCVD at 475°C results in CuPt ordering even at Sb concentrations as low as x = 0.07-0.14. The two $\{111\}_B$ variants are present, but each exists separately in 1-2 μm regions. However, the ordering is incomplete: it occurs in platelet domains lying on {111} habit planes within a disordered matrix, and is not continuous at the atomic scale within the domains. This ordering apparently explains the reduction in infrared emission energies relative to the bandgaps of bulk alloys. Similar ordering is found in an $InAs_{0.91}Sb_{0.09}/In_{0.87}Ga_{0.13}As$ strained-layer superlattice with lower-than-expected emission energy. High-resolution images indicate that the SLS has planar, sharply defined interfaces. Infrared LEDs have been made from such superlattices.

DISCLAIMER

This report was prepared as an account of work sponsored by an agency of the United States Government. Neither the United States Government nor any agency thereof, nor any of their employees, makes any warranty, express or implied, or assumes any legal liability or responsibility for the accuracy, completeness, or usefulness of any information, apparatus, product, or process disclosed, or represents that its use would not infringe privately owned rights. Reference herein to any specific commercial product, process, or service by trade name, trademark, manufacturer, or otherwise does not necessarily constitute or imply its endorsement, recommendation, or favoring by the United States Government or any agency thereof. The views and opinions of authors expressed herein do not necessarily state or reflect those of the United States Government or any agency thereof.

MASTER

DISTRIBUTION OF THIS DOCUMENT IS UNLIMITED

Introduction

In(As,Sb) alloys have the lowest bandgaps of ternary III-V semiconductor alloys and are of interest for infrared emitters and detectors. In earlier work, our laboratory examined $InAs_{0.7}Sb_{0.4}$ alloys and strained-layer superlattices (SLSs) grown by metal-organic chemical vapor deposition (MOCVD) and molecular beam epitaxy (MBE) for long-wavelength (8-12 μm) applications [1]. The spectral response extended down to 100 meV, in part due to CuPt-type ordering of the alloys, as also seen in this system by others [2-4]. Our current work explores mid-wavelength (2-5 μm) infrared materials using alloys and SLSs with lower Sb content [5]. We find that the optical emission energies of our MOCVD and MBE materials [6] are systematically lower than the bandgaps obtained by others [7]. Ordering of the alloyed sublattice into the CuPt arrangement is known to lead to reduced bandgaps in this system [8], but has an ideal 1:1 metalloid ratio. We nonetheless have found such order at an Sb concentration of only $InAs_{0.86}Sb_{0.14}$ [5], which is apparently responsible for the reduced emission energies.

Here, we characterize the microstructures of $InAs_{0.86}Sb_{0.14}$ and $InAs_{0.93}Sb_{0.07}$ alloys with transmission electron microscopy (TEM) and show that both contain ordered material. Examination of the ordered domains indicates that they are incompletely ordered and lie within a disordered matrix; both features are consistent with the appearance of CuPt order in alloys with low Sb concentrations. We also examined these alloys with two-beam imaging conditions known to reveal phase separation, as seen in many other alloys [9,10]. We find only a fine-scale (~10 nm) modulated contrast that disappears with decreasing Sb content. This contrast is discussed in terms of current ideas for compound semiconductor alloys about phase separation due to immiscibility and local statistical fluctuations in composition [11]. Finally, we characterized a SLS also having lower emission energy than predicted from bulk alloy bandgaps, and find that the $InAs_{0.91}Sb_{0.09}$ layers in it also exhibit CuPt order.

Experimental

The alloys and SLS were grown on (001) InAs at 475°C at pressures of 625-640 torr and V/III ratios of 2-20 for a growth rate of 1.7 μm/hr. The photoluminescence (PL) energies were found to be insensitive to the V/III ratio. Concentrations were obtained by x-ray diffraction using both the (004) and (335) reflections to correct for the amount of strain relaxation achieved; the error is $\Delta x \approx \pm 0.01$. The PL from the $InAs_{0.86}Sb_{0.14}$ alloy peaked at 240 meV [6], instead of 310 meV as expected from other work [7]. Similarly, for $InAs_{0.93}Sb_{0.07}$ the PL peak was at 335 meV, whereas 370 meV is expected [12]. Our growth temperature is high enough to avoid the coarse phase separation into 24-50 nm platelets parallel to the growth surface that was demonstrated by Ferguson et. al. [13] for growth at ≤ 400°C.

A cross-section TEM specimen of the $InAs_{0.86}Sb_{0.14}$ alloy was prepared by cleaving the wafer along <110> and epoxying two alloy surfaces together with a 90° rotation to insure that one orientation would be [110] and include the CuPt ordering reflections, since order is observed only for $\{111\}_B$ planes. The exact orientation of the $InAs_{0.93}Sb_{0.07}$ alloy and the SLS were determined by etching the back of the InAs wafer with 1 ml H_2SO_4 + 10 ml H_2O_2 to identify the $\{111\}_B$ planes [14]; these specimens were glued to a Si wafer. All specimens were epoxied into a stack of Si wafer pieces, and a cylinder ultrasonically cored with its center on the interface of interest. The cylinders were epoxied into a 3 mm o.d. brass tube for mechanical support, and disks were sliced from the tube. The disks were mechanically thinned with a rotating wheel "dimpler" which was centered on the interface, using 1 μm diamond paste followed by 0.05 μm alumina. The thickness of the $InAs_{0.93}Sb_{0.07}$ alloy and the SLS could be monitored more closely because the Si at the interface transmits light when < 10 μm thick. Final thinning was done by

ion milling with Ar; in some cases, this was followed by milling briefly with I_2 vapor present to reduce the amount of In surface residue seen on the specimen before this treatment. The specimens were examined in a Philips CM20T microscope at 200 keV (0.27 nm resolution achievable).

$InAs_{0.86}Sb_{0.14}$ Alloy Layer

The $InAs_{0.86}Sb_{0.14}$ alloy layer (specimen CVD 1088-1f) showed clear evidence of strain relaxation by the cross-hatched pattern seen optically on the surface. Measurements with cross-section TEM images gave a thickness of 1.65 μm, but variations of 0.05 μm were seen over distances of about 2 μm along the surface, as seen in Figs. 1a and 2b. These thickness variations are apparently producing the contrast seen optically and result from strain relaxation. Numerous dislocation segments are present in the layer, as in the cross-section image in Fig. 1a. Strong contrast is seen at the layer/substrate interface and a high density of dislocations can be discerned in the enlarged view in Fig. 1b, as expected for relaxation of the layer by misfit dislocations.

Electron diffraction indicated the presence of CuPt order in an alloy layer on one of the two sides of the glue line, apparently the [110] orientation, and not for the other side, as expected for ordering on only the $\{111\}_B$ variants. Selected area diffraction patterns taken from areas <~1 μm in diameter showed the two expected variants, but their relative intensities varied from place to place. In some cases, only one variant was present, while if the selected area was moved by ~1 μm laterally along the layer, the other variant would become dominant, such as in Fig. 2a. Bright-field images obtained with diffracted beams having a reciprocal lattice vector with nonzero components along the $<1\bar{1}1>$ ordering directions showed darker lines lying on the corresponding $\{111\}_B$ habit planes, as seen in Fig. 2b. The right side of Fig. 2b produced the diffraction pattern in Fig. 2a with the stronger CuPt variant having its ordering direction perpendicular to the dark features. Linear features lying along the other $\{111\}_B$ ordering habit planes are seen in the left side of Fig. 2b; in diffraction patterns from this side the second variant is dominant. An approximate boundary between these two sets of features is indicated by a dashed line. Dark-field images were obtained with the ordering reflections; the domains were illuminated very weakly, but linear features lying on the {111} habit planes could be identified as expected.

We interpret the dark features in Fig. 2b to be ordered platelet domains seen edge-on. They are a few tens of nanometers thick with comparable separations between them and are embedded within a disordered matrix. The overall ordered structure then consists of regions 1-2 μm across containing platelets of one variant lying on the corresponding $\{111\}_B$ habit planes, with the two variants occurring in separate regions. The lack of uniform ordering throughout the layer is not unexpected since the ratio of Sb/As = 0.14/0.86 = 0.16, instead of 1.0 required for perfect, space-filling CuPt order. Ordering appears stronger in the platelets, and they may be enriched in Sb.

The absence of complete order is also indicated by a feature in high-resolution TEM images. The [110] lattice image in Fig. 3 shows the presence of CuPt order as {111} atomic planes with light/dark intensities alternating along the ordering direction (large arrows). As expected, a given region shows only one variant. However, the intensity modulations stop and start when given {111} atomic planes are examined along their length. Thus ordering within the platelet domains appears not to be continuous. The CuPt order can be accounted for at the low Sb concentration by ordered domains within a disordered matrix and by incomplete ordering within the domains.

The separation of the variants into micrometer-size regions is quite different from the ordered structure of $In_{0.5}Ga_{0.5}P$, which has the ideal composition for lattice-matched growth on GaAs and consists of adjacent lamella (~1 nm thick) of the two variants alternating along the growth direction [15]. Figure 2b exhibits an intriguing correlation that suggests an explanation for the separation of the two variants into different regions. Note that the approximate boundary between them intersects a dip on the surface. On either side of the dip, the surface is tilted from (001) toward the $\{111\}_B$ plane corresponding to the variant beneath it. It is known that such tilting enhances growth of ordered material of that variant [16]. The tilting of the surface results from strain relaxation by misfit dislocations, and is evidenced by the cross-hatched pattern in Nomarski optical images. We speculate that during growth, strain relaxation and tilting occur, and the tilted surface enhances growth of the corresponding $\{111\}_B$ variant, leading to separated regions with a single dominant variant. The separation would then ultimately result from lattice mismatch of the alloy with the substrate.

$InAs_{0.93}Sb_{0.07}$ Alloy Layer

The cross-hatched pattern was again seen optically on the surface of the $InAs_{0.93}Sb_{0.07}$ alloy layer (specimen CVD 1097-2c), indicating that relaxation had occurred. The layer thickness measured 1.7 μm in the [110] cross-section orientation, and had fewer dislocation segments within it. Dislocations were again seen at the alloy/substrate interface. When the specimen was tilted 35° to the [111] viewing direction, individual dislocations are resolved in a somewhat regular network, as seen in Fig. 4.

Electron diffraction also indicated CuPt ordering at this concentration, as seen in Fig. 5. The behavior was the same as that for the $InAs_{0.86}Sb_{0.14}$ alloy layer; both variants could be detected, but their relative intensities varied when the selected area for diffraction was moved by ~1 μm laterally along the layer. The ordering reflections were weaker for the lower concentration specimen, and therefore details of the ordered microstructure were not pursued further with this specimen.

The $InAs_{0.93}Sb_{0.07}$ alloy layer does differ from the $InAs_{0.86}Sb_{0.14}$ alloy layer in another way. In the $(2\bar{2}0)$ two-beam, bright-field in Fig. 1b, a contrast of finely spaced, wavy lines elongated in the growth direction is observed for the higher concentration. The contrast is modulated along the $[1\,\bar{1}\,0]$ direction (parallel to the growth surface). The spacings between the lines are irregular, but are of the order of 10 nm. We were unable to detect this contrast using $(2\bar{2}0)$ two-beam, bright-field and dark-field images of the lower concentration alloy; it is not seen in Fig. 6. Such contrast has previously been interpreted as phase separation into two compositions separated by such spacings [10]. Recently, however, Glas [11] has proposed that such contrast could instead be due to fluctuations in local bond lengths caused by statistical variations in the near-neighbor alloy configurations for random alloys. The disappearance of the contrast (not seen in binary III-V compounds) at low alloy concentrations is consistent with either mechanism. Detailed examination of diffraction patterns from the $InAs_{0.93}Sb_{0.07}$ alloy shows the presence of diffuse scattering around the zincblende reflections and the appearance of diffuse streaks passing through these reflections along the $<1\,\bar{1}\,1>$ directions; Glas' computations [11] also indicate the presence of such diffuse scattering in electron diffraction patterns for random alloys.

It is noteworthy that ordering is clearly detected in the $InAs_{0.93}Sb_{0.07}$ alloy, whereas phase separation is absent. Since a reduced emission energy is found for this alloy, it is likely due to the presence of ordering. This result suggests that the ordering is probably the cause of the reduced energies in the higher Sb alloy, $InAs_{0.86}Sb_{0.14}$. The fine-scale modulations seen in this alloy (Fig. 1b) may be due to

either statistical fluctuations in a random alloy or phase separation, but phase separation is not required to explain the reduced emission energy.

Strained-Layer Superlattice

The above work demonstrates that MOCVD growth of $InAs_{1-x}Sb_x$ alloys at 475°C gives CuPt ordering, which is probably responsible for the reduced emission energies observed. The infrared devices envisioned for this system have active layers that are a SLS composed of alternating layers of $InAs_{1-x}Sb_x/In_{1-y}Ga_yAs$. This system is chosen because it can be grown lattice-matched to InAs and its compositions allow the 2-5 wavelength range to be spanned. The SLS configuration also strains the $InAs_{1-x}Sb_x$ emitting layers and thereby reduces the non-radiative recombination due to Auger processes [12]. A SLS of $InAs_{0.91}Sb_{0.09}/In_{0.87}Ga_{0.13}As$ has been used to make an LED with an output power of 0.02 W/cm^2 when operated at 77 K [5]. Details of the growth techniques, doping and x-ray characterization of the SLSs are also given in [5]. The optical emission energies of the devices are ~50 meV lower than expected from bandgap values obtained by others [6,7].

To address emission energies of the SLS directly, we used cross-section TEM to examine ordering in a structure of $InAs_{0.91}Sb_{0.09}/In_{0.87}Ga_{0.13}As$ with layer thicknesses of 9.0/13.0 nm as determined by fitting x-ray diffraction peaks (specimen CVD 1172-2e). A [110] electron diffraction pattern from a 1 μm-diameter area of the SLS is shown in Fig. 7. Very weak CuPt ordering reflections are seen for both variants. We were also able to detect order in lattice images of the thinner, $InAs_{0.91}Sb_{0.09}$ layers. Order was seen in isolated regions ~25 nm wide that contained only one variant. Thus the ordered structure in the SLS is very similar to that seen in the alloy layers discussed above.

The structure of the SLS was also characterized with TEM. Figure 8 shows the [110] cross-section image obtained with $(2\bar{2}0)$ two-beam, bright-field conditions. Some dislocations are seen in the InAs substrate and in the SLS. However, specimen preparation influenced the dislocation structure; after a second ion milling with I_2 to remove In residue, the dislocation structure was altered in regions previously characterized. The thinnest regions at the edge of the hole show more damage. It is notable that in some areas, the SLS/substrate interface shows no dislocations (right side of Fig. 8), implying that lattice matching has been reasonably well achieved. X-ray studies [5] indicate that the residual lattice mismatch is $\Delta a/a = 0.0016$.

The $(2\bar{2}0)$ two-beam image in Fig. 8 shows modulated contrast on a coarser scale: wavy features elongated in the growth direction with spacings of 50-100 nm. These features were not seen in the alloy layers discussed above, and indicate that phase separation like that in (In,Ga)(As,P) [10] and (In,Ga)P [9] has occurred. Bangert et al. [17] find such contrast modulation in layered structures which they ascribe to phase separation based upon the average concentration at the layer interfaces. In our SLS, phase separation might then be induced by the $In_{0.87}Ga_{0.13}As$ layers' interacting with the $InAs_{0.91}Sb_{0.09}$ layers, since the latter show no such contrast in thick alloy layers.

Figure 9a shows a section of the SLS, imaged in bright-field with (004) two-beam condition. The individual layers are sharp and straight. By counting atomic planes across the layers in lattice images and using $a_0 = 0.60584$ for InAs, the superlattice period was determined to be 22.7±0.5 nm. When electron diffraction patterns are taken with highly parallel incident electron beams (more so than in Fig. 7), finely spaced satellites are observed on either side of the zincblende reflections along [001], as seen in Fig. 9b. The spacing of the satellites also indicates the superlattice period, 23.0±0.5 nm, in good

agreement with the lattice image. The fifty-period SLS then has a total thickness of 1.15 μm. However, lattice imaging gives a greater thickness for the thinner layer than found with x-ray analysis, 10.6±0.05 nm; the second layer is then 12.1±0.5 nm thick, about 1 nm less than found with x-rays. The superlattice period differs by only 0.7 nm from the x-ray value.

Conclusions

$InAs_{1-x}Sb_x$ alloys grown by MOCVD at 475°C contain CuPt ordering even at Sb concentrations as low as x = 0.07. The ordering consists of the expected two $\{111\}_B$ variants, but each variant occurs separately in 1-2 μm regions. The separation contrasts strongly with ordering in $In_{0.5}Ga_{0.5}P$ alloys, where the two variants are interspersed as ~1 nm lamella [15]. This ordering apparently explains the reduction in infrared emission energies relative to the bandgaps of bulk alloys. However, the ordering is incomplete, as expected from the non-ideal alloy composition. Ordering appears to occur in domains within a disordered matrix, and within the domains, ordering is not continuous at the atomic scale.

It is widely accepted that ordering is produced on the surface during growth [18]. While a detailed understanding of the mechanism is not available and would probably vary for different alloys, CuPt order generally requires preferential placement of atoms into two alternating sites. The two sites might be tensile and compressive locations on a reconstructed surface, for instance, with preferences for larger and smaller atoms, respectively. The occurrence of order for x = 0.07 indicates that the two types of sites are present at such low Sb concentrations.

Very similar ordering is found in an $InAs_{0.91}Sb_{0.09}/In_{0.87}Ga_{0.13}As$ SLS and apparently also explains its lower-than-expected emission energy. High-resolution images indicate that the SLSs are of high quality with planar, sharply defined interfaces. These SLSs are being used to make infrared LEDs [5], but their output may be limited by residual lattice mismatch with the substrate and resulting misfit dislocations that allow non-radiative recombination. The SLSs have also been shown to lase [19], and electrically injected lasers are anticipated based on these structures.

Acknowledgements

The authors would like to thank M. P. Moran for preparing cross-section TEM specimens and M. W. Pelczynski for assistance with the MOCVD growth. Comments on the work by J. Olsen and G. B. Stringfellow were quite useful. This work done at Sandia National Laboratories was supported by the U. S. Department of Energy under Contract DE-AC04-94AL85000.

References

1. S. R. Kurtz, L. R. Dawson, R.M. Biefeld, D. M. Follstaedt and B. L. Doyle, Phys. Rev. **B46**, 1909 (1992).

2. Y.-E. Ihm, N. Otsuka, J. Klem and H. Morkoc, Appl. Phys. Lett. **51**, 2013 (1987).

3. J. R. Yen, K. Y. Ma and G. B. Stringfellow, Appl. Phys. Lett. **54**, 1154 (1989).

4. T-Y. Seong, A. G. Norman, G. R. Booker, R. Droopad, R. L. Williams, S. D. Parker, P. D. Wang and R. A. Stradling, Mat. Res. Soc. Symp. Proc. **163**, 907 (1990).

5. R. M. Biefeld, K. C. Baucom, S. R. Kurtz and D. M. Follstaedt, Mat. Res. Soc. Symp. Proc. **325**, 493 (1994).

6. R. M. Biefeld, K. C. Baucom and S. R. Kurtz, J. Crystal Growth **137**, 231 (1994).

7. Z. M. Fang, K.Y. Ma, D.H. Jaw, R.M. Cohen and G.B. Stringfellow, J. Appl. Phys. **67**, 7034 (1990).

8. S-H. Wei and A. Zunger, Appl. Phys. Lett. **58**, 2684 (1991).

9. D. M. Follstaedt, R. P. Schneider, Jr., and E. D. Jones, submitted to Journal of Applied Physics.

10. T. L. McDevitt, S. Mahajan, D. E. Laughlin, W. A. Bonner and V. G. Keramidas, Phys. Rev. **B45**, 6614 (1992).

11. F. Glas, Inst. Phys. Conf. Series **134**, 295 (1993).

12. S. R. Kurtz, R. M. Biefeld and L. R. Dawson, submitted to Applied Physics Letters.

13. I. T. Ferguson, A. G. Norman, B. A. Joyce, T-Y. Seong, G. R. Booker, R. H. Thomas, C. C. Phillips and R. A. Stradling, Appl. Phys. Lett. **59**, 3324 (1991).

14. P. D. Warren, The Relation Between Electronic and Mechanical Properties of Non-Metals, Ph.D. Thesis, Trinity College (Oxford, England, 1987), p. 36.

15. C. S. Baxter, W. M. Stobbs and J. H. Wilkie, J. Crystal Growth **112**, 373 (1991).

16. G. S. Chen and G. B. Stringfellow, Appl. Phys. Lett. **59**, 3258 (1991).

17. U. Bangert, A. J. Harvey, V. A. Wilkinson, C. Dieker, J. M. Jowett, A. D. Smith, S. D. Perrin and C. J. Gibbins, J. Crystal Growth **132**, 231 (1993).

18. A. Zunger and S. Mahajan, in Handbook on Semiconductors, **3**, 2nd ed. (Elsevier, Amsterdam, 1993).

19. S. R. Kurtz, R. M. Biefeld, L. R. Dawson and K. C. Baucom, Appl. Phys. Lett. **64**, 812, (1994).

Figure Captions

Figure 1. $InAs_{0.86}Sb_{0.14}$ alloy layer view tilted a few degrees from [110] and imaged with $(2\bar{2}0)$ two-beam condition in bright field. a) Dislocation segments are seen threading across the layer, and strong contrast (dark) is seen at the alloy/substrate interface. The two bars indicate positions of the front surface/glue interface and demonstrate that the thickness of the alloy layer varies with position. b) Higher magnification shows numerous dislocations at the interface. A mottled contrast of fine wavy lines running near perpendicular to the growth surface is also seen.

Figure 2. a) [110] electron diffraction pattern obtained from the $InAs_{0.86}Sb_{0.14}$ alloy layer using a selected area 1 μm in diameter. Spots due to both variants can be seen (arrowed), but one is noticeably stronger. b) Bright field image near [110] orientation. The center and right side of the figure show darker linear features (arrowed) lying on the $(1\,\bar{1}\,1)$ habit plane; this region correlates with the strong variant seen in a). The left side shows similar features (arrowed) lying on the $(\bar{1}\,1\,1)$ habit plane corresponding to the other variant. Dashed line shows the approximate boundary between the two regions.

Figure 3. [110] lattice image of the $InAs_{0.86}Sb_{0.14}$ alloy layer in a region containing one variant. The presence of ordering is seen by looking along the $(\bar{1}\,1\,1)$ planes (large arrows) and noting the light/dark intensity of the planes alternating in the $[\bar{1}\,1\,1]$ direction (separation = $2xd_{(111)}$ = 0.7 nm). Although the difference is weak, it is significant, which can be appreciated by looking along the $(1\,\bar{1}\,1)$ planes of the non-ordered variant (small arrows). The modulated intensity along the ordered planes starts and stops, indicating that ordering is not uniform within domains.

Figure 4. Image showing a network of dislocations at the $InAs_{0.93}Sb_{0.07}$ alloy layer/substrate interface, obtained by tilting the [110] cross-section specimen to [111] orientation and imaging with $(2\bar{2}0)$ two-beam condition in bright field.

Figure 5. [110] electron diffraction pattern obtained from the $InAs_{0.93}Sb_{0.07}$ alloy layer using a selected area 1 μm in diameter. Both variants (long arrows) are seen. Other weak spots (short arrows) are due to In residue on the specimen surface.

Figure 6. Bright-field, $(2\bar{2}0)$ two-beam image of $InAs_{0.93}Sb_{0.07}$ alloy layer. Fine-scale contrast modulations like those in Fig. 1b) is not detected here. The dark spots are In residues.

Figure 7. [110] electron diffraction pattern from $InAs_{0.91}Sb_{0.09}/In_{0.87}Ga_{0.13}As$ SLS, showing weak CuPt ordering reflections from the two $\{111\}_B$ variants and wavy streaks between them along [001].

Figure 8. [110] cross-section image of $InAs_{0.91}Sb_{0.09}/In_{0.87}Ga_{0.13}As$ SLS on InAs substrate obtained with $(2\bar{2}0)$ two-beam, bright-field condition. Dark horizontal lines within the SLS are dislocations. Lower-contrast, wavy features elongated in the growth direction are due to phase separation.

Figure 9. a) [110] cross-section image of part of the $InAs_{0.91}Sb_{0.09}/In_{0.87}Ga_{0.13}As$ SLS obtained with (004) two-beam condition in bright field. b) [110] electron diffraction pattern containing central beam and four {111} zincblende reflections, taken with highly parallel illumination to resolve satellites on either side of those reflections along the [001] direction.

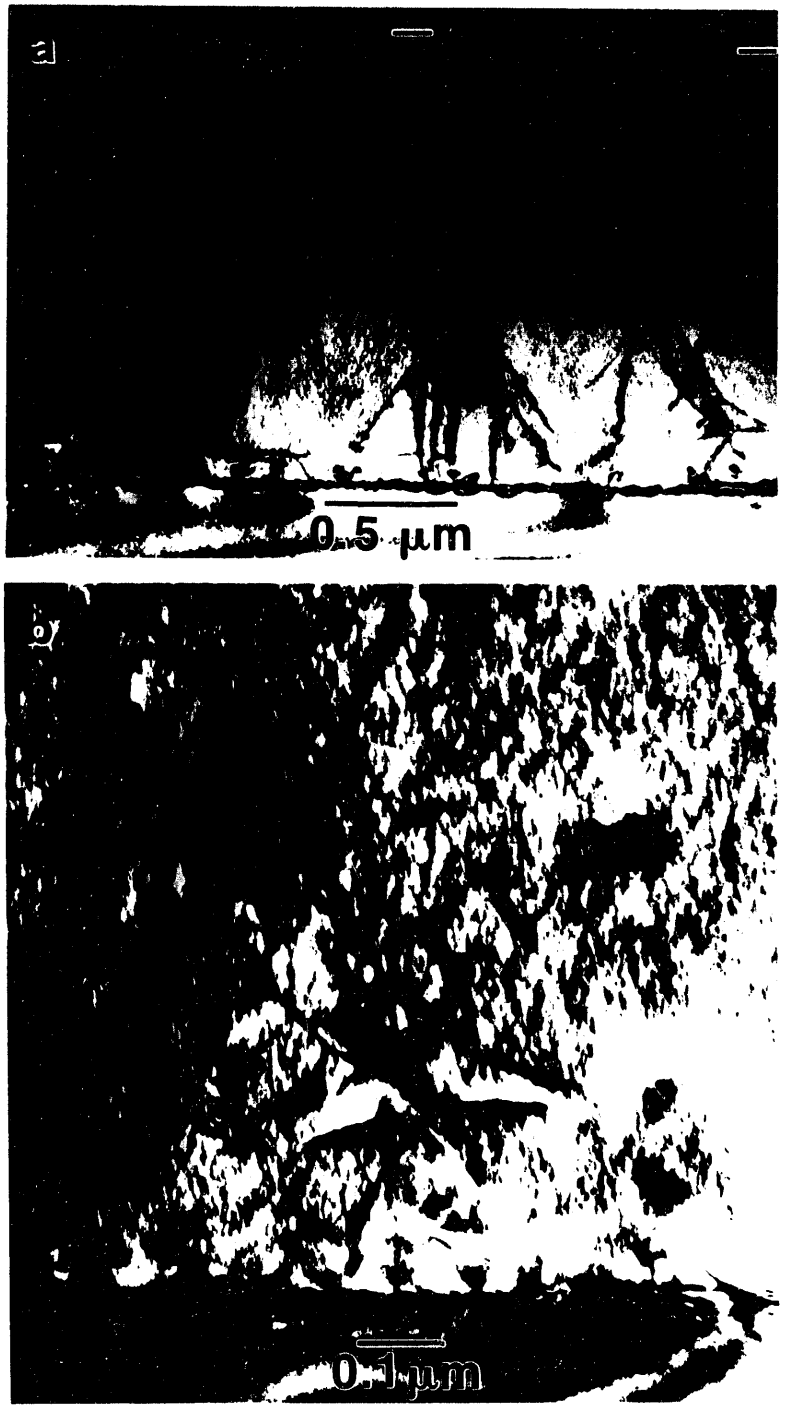
a)
0.5 μm
b)
0.1 μm

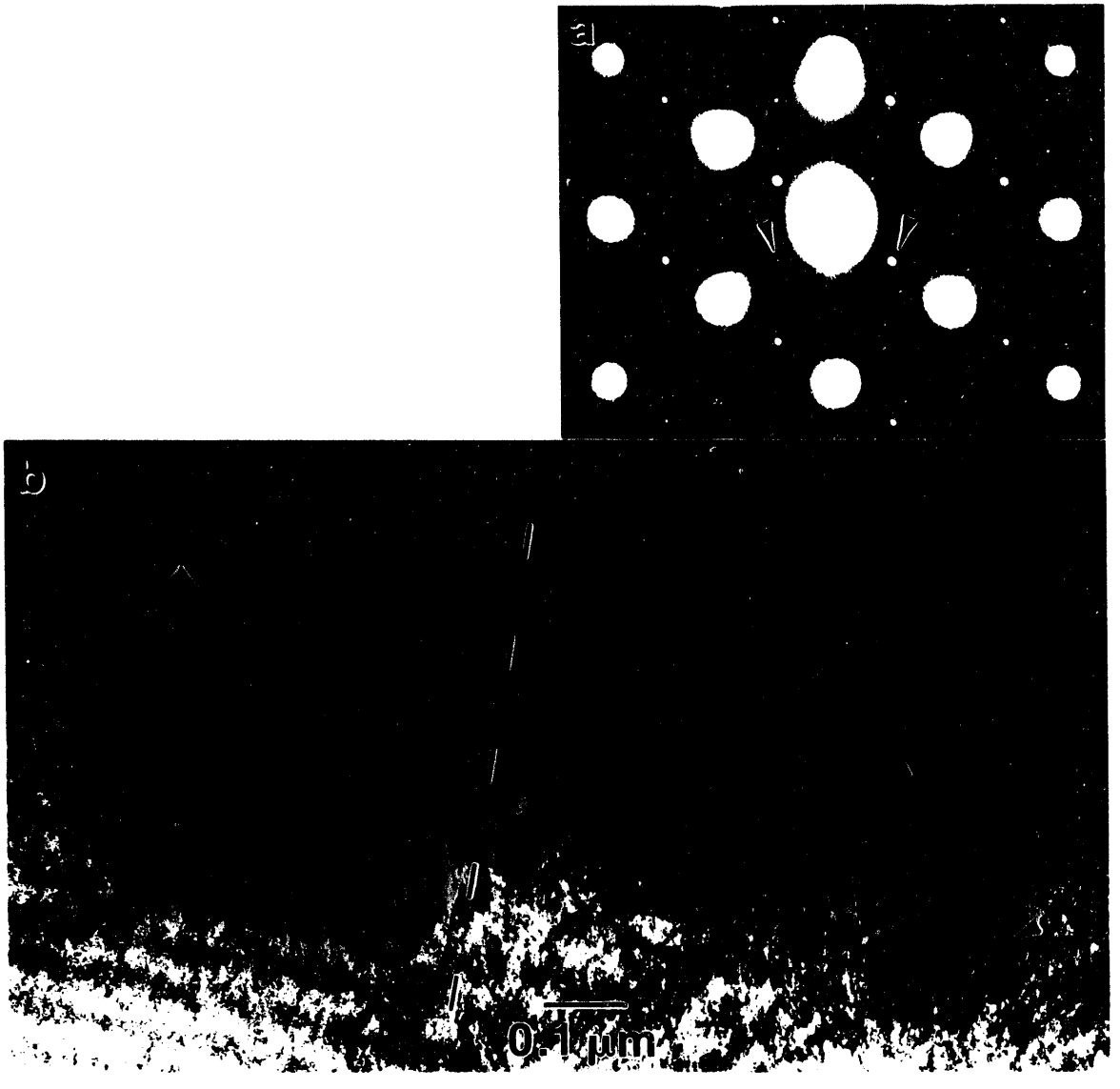
a)
b)
0.1 μm

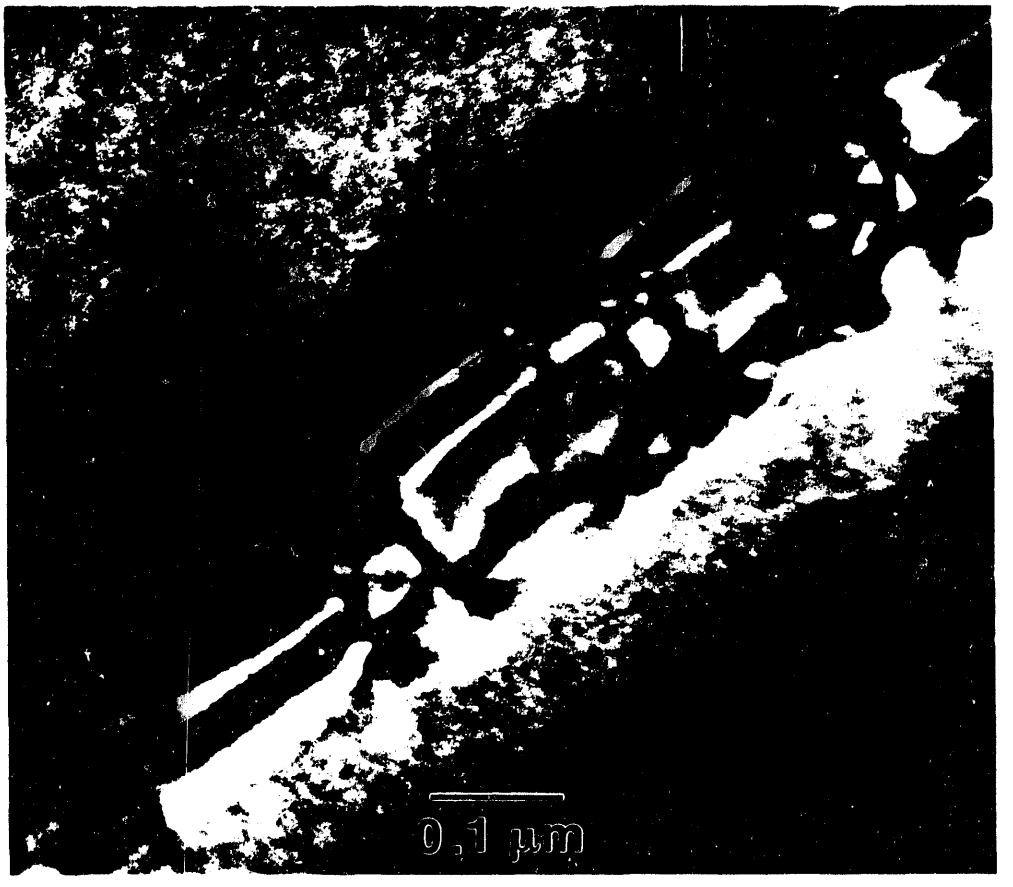
0.1 μm

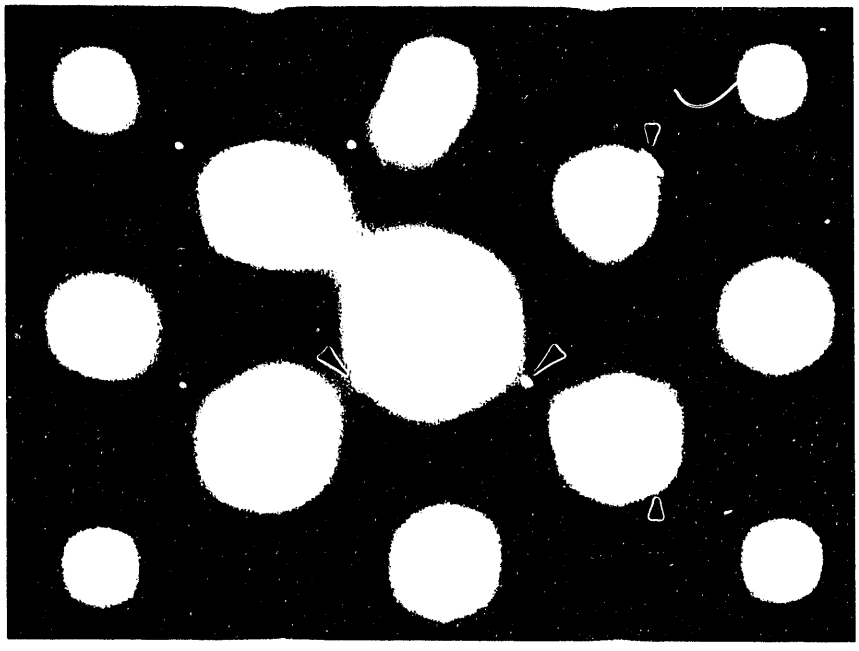


[001]
0.1μm

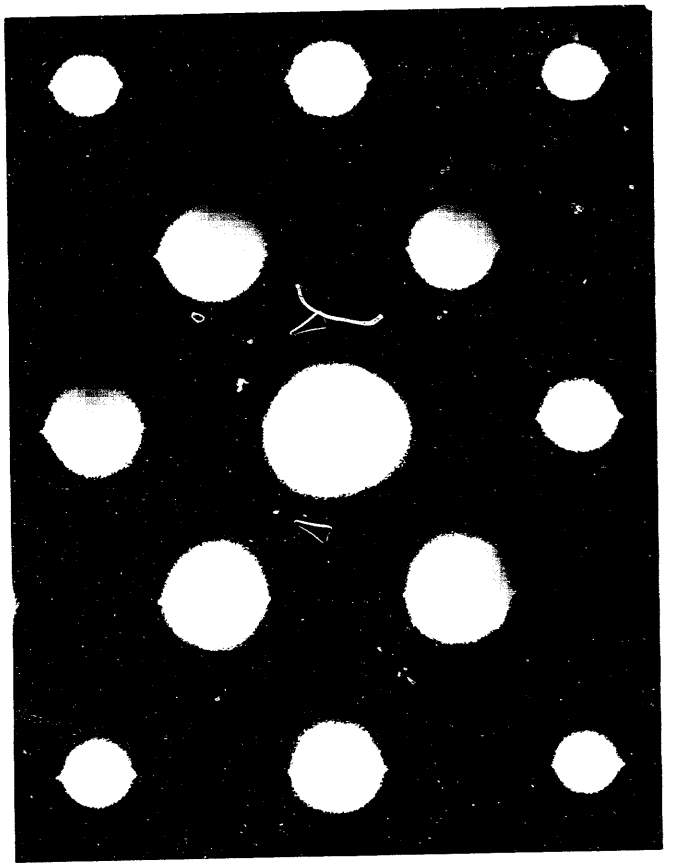

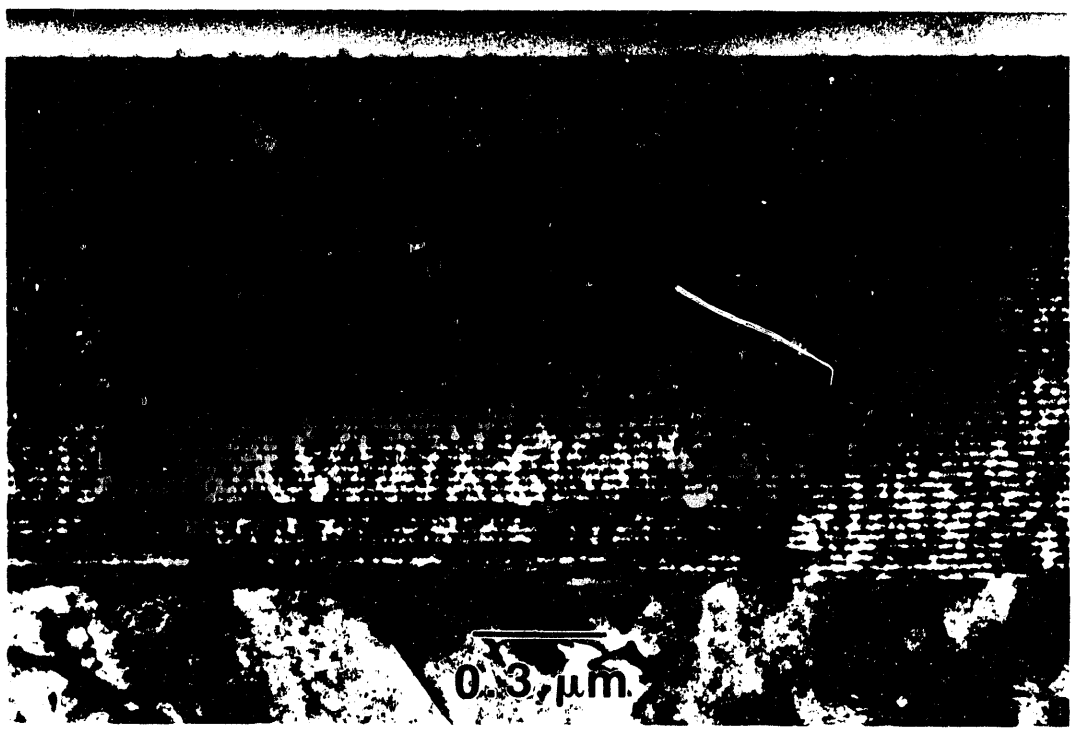
0,3 µm.

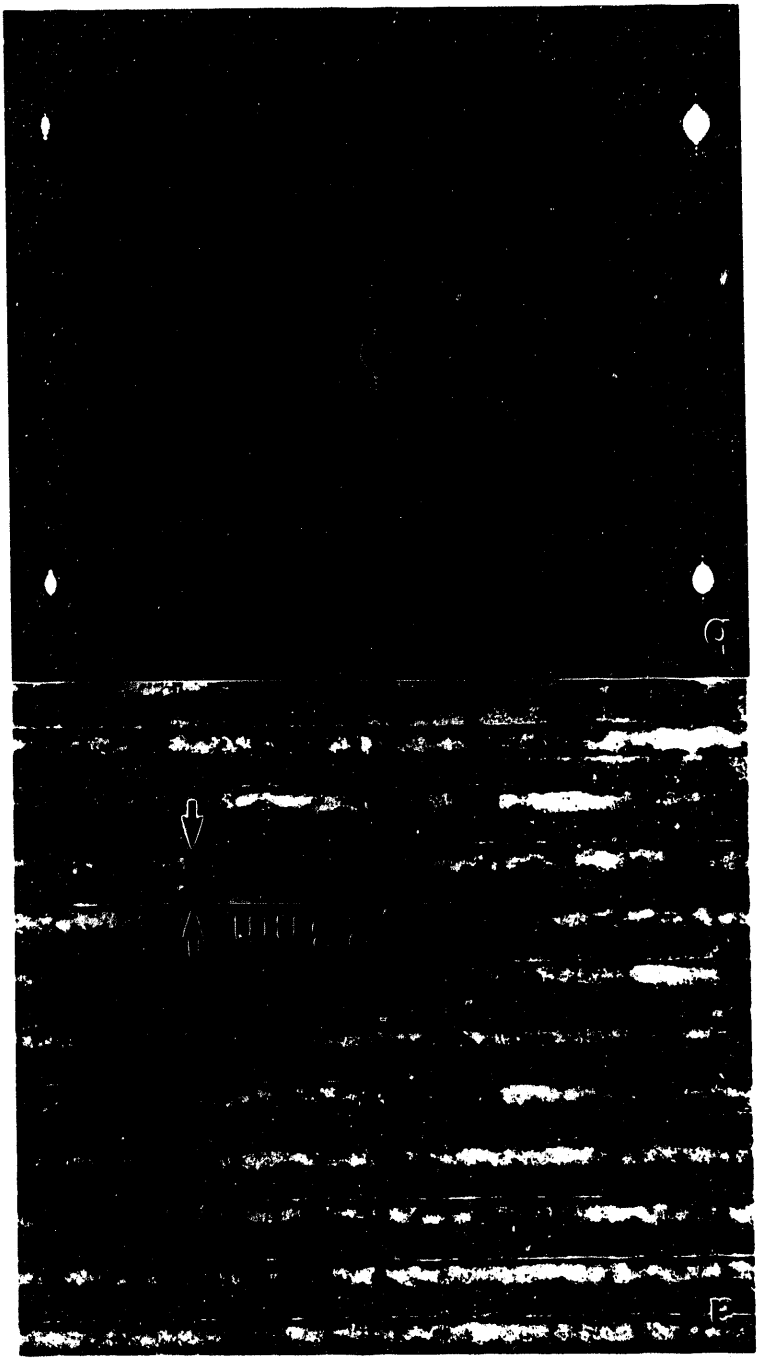

DATE
FILMED
9/6/94
END